A MODEL FOR ULTRASOUND TRANSMISSION THROUGH GRAPHITE COMPOSITE PLATES CONTAINING DELAMINATIONS

F. J. Margetan, T. A. Gray, R. B. Thompson, and
B. P. Newberry

Center for NDE
Iowa State University
Ames, IA 50011

INTRODUCTION

The propagation of elastic waves through materials and their interactions with flaws are fundamental phenomena underlying many nondestructive evaluation techniques. Over the past decade, considerable research has led to a good understanding of these phenomena for isotropic materials. For example, it is now possible to predict the absolute signals that will be observed when flaws of simple shapes, e.g., circular cracks or spherical pores, are examined in an immersion test through planar or cylindrically curved surfaces [1]. These models have now been used to successfully predict the probability of detection (POD) [2], an important figure of merit of a practical inspection, and it has been suggested that this capability will find important applications in a) the validation of existing NDE techniques, b) the design of new NDE techniques, or c) the consideration of inspectablility in part design [3,4].

Considerably less work has been done in anisotropic materials. Results of some early work are found elsewhere in these proceedings [5]. The present paper addresses the problem of modeling the through transmission inspection of a graphite composite plate containing delaminations. As in the previous work by the authors in isotropic media [1], an electromechanical reciprocity relation [6] is used to provide the formal structure for the calculations. Various beam models are then combined with a Kirchhoff approximation for the scattering to predict the through transmitted signals. Here the philosophy is to seek a simple model, employing a number of approximations, which will allow the primary variables observed in a practical experiment to be predicted with modest computational effort. The accuracies of the various model approximations are assessed by comparison to experiments in a series of quasi-isotropic, graphite-epoxy, laminated plates. The utility of the present model, and possible refinements, are discussed in the concluding section.

MODEL OVERVIEW

Our theoretical approach is based on Auld's general reciprocity formula [6] which relates ultrasonic fields in the vicinity of a flaw to electromagnetic (EM) signals in the transducer cables. Figure 1 depicts our through-transmission inspection geometry and our model

coordinate system. Co-axial cable a transports input electrical energy toward transmitting transducer A. A portion of this energy is converted to ultrasound, which propagates past the flaw to receiving transducer B. Some of the received ultrasound is converted to electrical energy, appearing as an EM wave propagating to the right in co-axial cable b.

We consider a steady-state situation characterized by harmonic oscillations with time dependence $e^{i\omega t}$, $\omega=2\pi f$. At points sufficiently far removed from transducer A, the EM field within cable a is a superposition of fundamental mode incident and reflected fields. The time-averaged electrical power carried by the incident field toward transducer A is denoted P. The outgoing EM field in cable b can be described by a dimensionless overall transmission coefficient Γ. This is done by writing the electric and magnetic fields within cable b as $E=\Gamma E_p$ and $H=\Gamma H_p$; here the reference fields (E_p,H_p) are the fundamental-mode fields for cable b which transport power P to the right in Fig. 1. Thus, electrical power P is incident upon transducer A, and power $\Gamma^2 P$ is output by transducer B.

For nonpiezoelectric elastic media, Auld has derived a relationship for the change in Γ induced by the flaw. This may be written

$$\Gamma_{flaw} - \Gamma_{n.f.} = -(1/4P) \int_{S_-+S_+} [\mathring{u}^a \cdot T^b - \mathring{u}^b \cdot T^a] \cdot \hat{n} dS. \qquad (1)$$

Here Γ_{flaw} denotes the transmission coefficient for the situation shown in Fig. 1, and $\Gamma_{n.f.}$ denotes the coefficient for the same geometry when no flaw is present. The integration is over any closed surface containing the flaw. For the case of a delamination to be considered here, we choose to integrate over its physical surfaces (S_-+S_+). $\hat{n}$ is an outward unit normal vector to this surface. $\mathring{u}^a$ and T^a are the time independent factors of the velocity and stress fields produced in the presence of the flaw when transducer A is excited by incident electrical power P. $\mathring{u}^b$ and T^b are the fields which would be produced in the absence of the flaw when transducer B is excited by incident power P. The precise definitions of the inner product "$\cdot$" notation, and the (generally complex) power P are given by Auld [6].

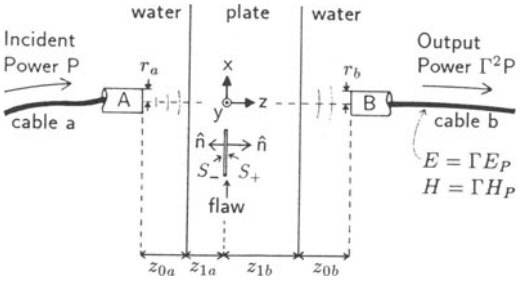

Fig. 1. Inspection geometry and model coordinate system. x,y, and z are assumed to be principal axes of the graphite composite plate.

When the flaw is a void, such as a delamination, the stress must vanish on the flaw surface; hence $T^a \cdot \hat{n} = 0$ in Eq. (1). When the delamination is thin compared to a wavelength, it is straightforward to rewrite the remaining term as an integral over the illuminated face:

$$\Gamma_{flaw} - \Gamma_{n.f.} = (1/4P) \int_{S_-} \Delta\dot{u}^a \cdot T^b \cdot \hat{n} dS \qquad (2)$$

Here $\Delta\dot{u} \equiv \dot{u}(z=0^+) - \dot{u}(z=0^-)$ is the change in particle velocity across the thickness of the delamination.

If the delamination filled the entire xy plane in Fig. 1, no ultrasound would reach transducer B. For such a flaw, Eq. (2) becomes

$$0 - \Gamma_{n.f.} = (1/4P) \int_{xy\ plane} \Delta\dot{u}^a \cdot T^b \cdot \hat{n} dS. \qquad (3)$$

Dividing Eq. (2) by Eq. (3) leads to

$$\Gamma_{flaw}(f)/\Gamma_{n.f.}(f) = 1 - \int_{S_-} \Delta\dot{u}^a \cdot T^b \cdot \hat{n} dS \Big/ \int_{xy\ plane} \Delta\dot{u}^a \cdot T^b \cdot \hat{n} dS \qquad (4)$$

Because of the manner in which Γ is defined, the ratio of transmission coefficients on the l.h.s. of Eq. (4) is equal to the corresponding ratio of received voltages in cable b, as long as the equipment is operating in a linear regime. Note that the $\Delta\dot{u}$ terms in the numerator and denomination of Eq. (4) are associated with different flaws, and hence need not be identical at overlapping points. However, certain cancellations will still occur to simplify the evaluation of the r.h.s. of Eq. (4); e.g., the effects of equipment power levels and transducer efficiencies will exactly cancel. Also notice that Eq. (3) will hold true for any plane-filling delamination regardless of its location within the plate. Thus, the value of the integral in the denominator of Eq. (4) is independent of z_{1a}(for fixed $z_{1a} + z_{1b}$), a fact that can be used to check the evaluation of this integral.

MODEL APPROXIMATIONS

When evaluating the r.h.s. of Eq. (4) for a particular experimental arrangement, we make the following approximations.

i) Each composite plate is treated as an orthorhombic homogeneous medium, characterized by, at most, nine independent elastic constants [7]. We treat the plate as either an anisotropic or an isotropic medium. For the anisotropic treatment we retain the full set of elastic constants. For the isotropic treatment, we use only the speeds of sound in the forward (z) direction to determine the two independent constants. By comparing the results of these two treatments we can gauge the importance of the anisotropy.

ii) Ultrasonic attenuation is not explicitly modeled. The effects of attenuation are assumed to largely cancel in the ratio of integrals.

iii) To propagate a transducer's radiation field through water and through unflawed, nonattenuating solid we use one of three beam models. For isotropic treatments of the composite we use either the Gaussian (G) beam model of Thompson and Lopes [8] or the Gauss-Hermite (GH) beam model of Thompson et al. [9]. For anisotropic treatments we employ a recent extension of the Gaussian beam model formulated by Thompson and Newberry [5].

iv) The inspection process being modeled utilizes longitudinal waves propagating in the z-direction. When evaluating the integrands in Eq. (4), we assume that the z-component of particle motion and derivatives with respect to z dominate the x and y components. A full expression for the integrand in our principal axis coordinate system is

$$\Delta\hat{u}^a \cdot T^b \cdot \hat{n} = -[\Delta\hat{u}_1^a C_{55}(u_{1,3}^b + u_{3,1}^b) + \Delta\hat{u}_2^a C_{44}(u_{2,3}^b + u_{3,2}^b) \qquad (5)$$

$$+ \underline{\Delta\hat{u}_3^a (C_{33} u_{3,3}^b + C_{31} u_{1,1}^b + C_{32} u_{2,2}^b)} \;].$$

Here $,i \equiv \partial/\partial x_i$ and we have used abbreviated subscript notation for the elastic constants. We retain only the underlined term in Eq. (5). Moreover, we note that the variation of u_3^b with z is dominated by the phase factor $e^{ik_3 z}$, and we approximate $u_{3,3}^b = \partial u_z^b/\partial z$ by $ik_3 u_3^b$.

v) A Kirchhoff approximation is used for the scattering of the incident field by the delamination. The far side of the delamination (S_+) is considered to be "dark", and a local plane wave reflection analysis is used to determine the total field on the illuminated side (S_-). For near normal incidence this leads to $\Delta\hat{u}_z^a = -2\, u_z^{a,inc}$ where "inc" denotes the incident field.

Using these approximations, Eq. (4) can be rewritten as

$$\Gamma_{flaw}(f)/\Gamma_{n.f.}(f) = 1 - \int_{S_-} \hat{u}_z^{a,inc} u_z^{b,inc} dS \Big/ \int_{xy\ plane} \hat{u}_z^{a,inc} u_z^{b,inc} dS \qquad (6)$$

where the incident fields from each transducer are obtained from one of the three beam models.

EXPERIMENTAL PROCEDURE

The most rigorous tests of the model will occur when the lateral dimensions of the flaw and interrogating beam are comparable. When planar transducers are used, our Gaussian beam model approximations are expected to be most accurate in the far field [8], i.e., when $s \equiv (\lambda_o z_o + \lambda_1 z_1)/r^2 >> 1$ for each transducer in Fig. 1. For focussed transducers, the approximations should be best near the focal plane. So that we could work with larger and more easily manufactured flaws, we chose to use planar transducers in our initial experiments. In particular, we used matched 1/4" (.635cm) diameter probes having nominal center frequencies of 10MHz. The transmitting probe was excited by a sharp electrical pulse, producing a broadband ultrasonic signal with a useful spectral amplitude between $2MHz < f < 16MHz$. Ten centimeter waterpaths were used on each side of the plate, resulting in $s = 16/(f \text{ in MHz})$.

Graphite composite plates supplied to us by LTV Aerospace and Defense Corp. were approximately 0.8cm thick, and were formed from 64 layers of a "pre-preg" tape (AS-4/3502). Each tape layer consisted of uniaxial graphite fibers in an epoxy matrix, and the layers were symmetrically arranged parallel to the xy plane of Fig. 1. Measured w.r.t. the positive x-axis, fiber orientations for sequential layers were 0°, 0°, 90°, 90°, +45°, +45°, -45°, -45°, 0°, 0°, ... This layup resulted in a "quasi-isotropic" sample with approximate rotational symmetry about the z-axis of Fig. 1. Seeded defects consisted of double layers of thin teflon tape in the shape of circles (1/8" (.318cm) and 1/4" (.635cm) in diameter) or strips (3/16" x 4" = .476cm x 10.2cm). Five defects of each type were inserted into our set of sample plates during manufacture. Some defects were simply placed between the 33rd and 34th layers; others were inserted into matching holes cut in the 33rd layer.

The following procedure was used to acquire experimental through-transmission signals for comparison with theory. With the plate removed, the two probes were aligned for coaxial beams by maximizing the high frequency component (f>15MHz) of the received signal. The plate was then inserted, and its front surface reflection was maximized to align the plate perpendicular to the beam. For arbitrary, but fixed, settings of the equipment gain controls, we then recorded the received voltage (V) in cable b as a function of time, averaged over 64 pulses. This was done for transmissions through flawed [$V_{flaw}(t)$] and unflawed [$V_{n.f.}(t)$] portions of the plate. These time domain signals were then Fourier transformed to obtain their frequency spectra, $V_{flaw}(f)$ and $V_{n.f.}(f)$, respectively. The complex experimental ratio $V_{flaw}(f)/V_{n.f.}(f)$ can be directly compared with the theoretical ratio $\Gamma_{flaw}(f)/\Gamma_{n.f.}(f)$. A second method of comparison uses the measured reference signal and theory to predict the time-domain signal received when a flaw is present:

$$V_{flaw}^{predicted}(t) = \text{I.F.T.} \left[V_{n.f.}(f) \left(\Gamma_{flaw}(f)/\Gamma_{n.f.}(f)\right) \right] \qquad (7)$$

The predicted flaw signal can then be directly compared with the observed time-domain flaw signal.

MODEL INPUTS AND CALCULATIONS

Inputs for the model evaluation of Eq. (6) are the oscillation frequency, the geometrical parameters in Fig. 1, material properties of water and the plate, and, for the Gauss-Hermite beam treatment, certain mathematical parameters which govern the convergence of the model results. The relevant geometrical inputs are $r_a=r_b=0.3175$cm, $z_{oa}=z_{ob}=10$cm, $z_{1a}=z_{1b}=0.4$cm, together with the dimensions and position of the delamination. The Gaussian beam models require the selection of an initial beam width parameter (W_o) at the face of the piston probe. We used $W_o=.7517r$ which results from fitting the Gaussian beam to the central lobe of the piston probe radiation pattern in the very far field ($s\to\infty$) [8]. Material properties required by the isotropic treatments are the densities [$\rho(\text{water})=1.0\text{gm/cm}^3$; $\rho(\text{solid})=1.6\text{gm/cm}^3$] and the speeds of sound in the z-direction [$v_L(\text{water})=.15\text{cm/}\mu\text{s}$; $v_L(\text{solid})=.31\text{cm/}\mu\text{s}$; $v_T(\text{solid})=.19\text{cm/}\mu\text{s}$)]. The anisotropic Gaussian beam treatment [5] additionally requires the dimensionless ratio

$$\Lambda_x/\lambda_z = \Lambda_y/\lambda_z = C_{55}/C_{33} + (C_{13}+C_{55})^2/C_{33}(C_{33}-C_{55}) \qquad (8)$$

which determines the modification of the rate of beam spread due to the anisotropy of the solid. (Λ/λ is unity for an isotropic material.) C_{13} was not accurately known for our plate samples, and we intentionally overestimated its value to arrive at $\Lambda_x/\lambda_z = 2$. This choice most likely overstates the effect of anisotropy on beam propagation.

The three beam models are compared in Fig. 2 at the nominal center frequency of the transducers. The Gauss-Hermite beam profile displays the side lobes typical of piston probe radiation patterns. The speed of sound for propagation in the xy plane of the plate is approximately twice that for propagation along the z axis. This anisotropy tends to accelerate the widening of the beam as it traverses the plate. However, Fig. 2 demonstrates that this additional widening is minimal for our experimental situation.

To permit the prediction of time-domain flaw signals using Eq. (7), Eq. (6) was evaluated at f=1/2, 1, 1 1/2, ..., 20MHz. The circular symmetry of the model beams was used to reduce the area integrals to one-dimensional radial integrals which were usually evaluated numerically. However, the denominator integral in Eq. (6) can be evaluated analytically for the Gaussian beam treatments. The evaluation of Eq. (6) typically required two seconds of DEC Microvax I cpu time per frequency for the Gaussian treatments, and 30 seconds per frequency for a fully-converged Gauss-Hermite treatment.

COMPARISON OF THEORY AND EXPERIMENT

Figure 3 illustrates the manner in which through-transmitted signals are modified by the presence of a delamination. As the beam sweeps toward the center of the flaw, we observe a reduction in signal amplitude

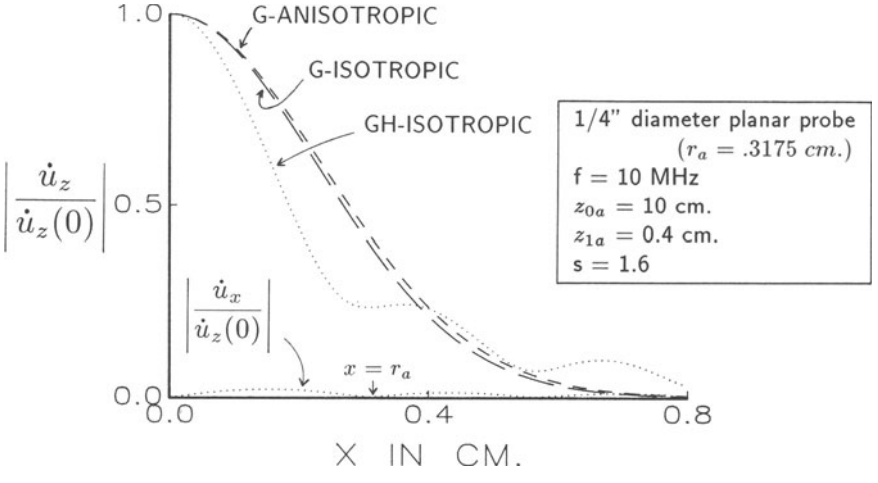

Fig. 2. Incident beam particle velocity profiles at the midplane of the composite plate, as predicted by the three beam models. Each curve has been scaled by dividing by $\mathring{u}_z(x=y=0)$, the model velocity on the beam axis. Each beam profile has rotational symmetry about the z-axis of Fig. 1. The bottommost curve displays the Gauss-Hermite model prediction of $\mathring{u}_x$; the approximation $\mathring{u}_x, \mathring{u}_y \ll \mathring{u}_z$ is used in the evaluation of Eq. (4).

and a selective blocking of the high frequency components. The experimental curves in Fig. 3 were obtained using one of the five seeded 1/4-inch (.635cm) diameter circular flaws. The theoretical curves were obtained from Eqs. (6) and (7), using the Gauss-Hermite beam model and the experimental no-flaw signal shown at the top of Fig. 3. The experimental signals are "stretched out" in time by the resonant reverberation of ultrasound between pairs of layers in the plate. Because the reverberation information is encoded in the no-flaw signal, reverberations also appear in the predicted flaw signals. Considering the simplicity of the model, the degree of agreement between theory and experiment in Fig. 3 is quite gratifying.

More-detailed comparisons of theory and experiment are shown in Figs. 4a-6a. There we display, as a function of frequency, the ratio of received voltages when a flaw is and is not present. For each flaw type and location, 5 to 20 experimental trials were conducted using different flaws and/or different reference signals. It was common to observe 10% variations in the amplitude of the reference signal when the beam was scanned through portions of a plate far from the seeded defects. Each error bar shown in Figs. 4a-6a encompasses ± one standard deviation of the individual experimental measurements from their mean.

Figure 4a is typical of situations in which the UT beam is centered on a delamination of comparable size to the beam itself. We observe a pronounced drop in voltage ratio with increasing frequency due to the narrowing of the beam. At high frequencies, the width of the beam approaches the physical width of the transducer and the voltage ratio becomes constant. Comparing the upper two theory curves in Fig. 4a,

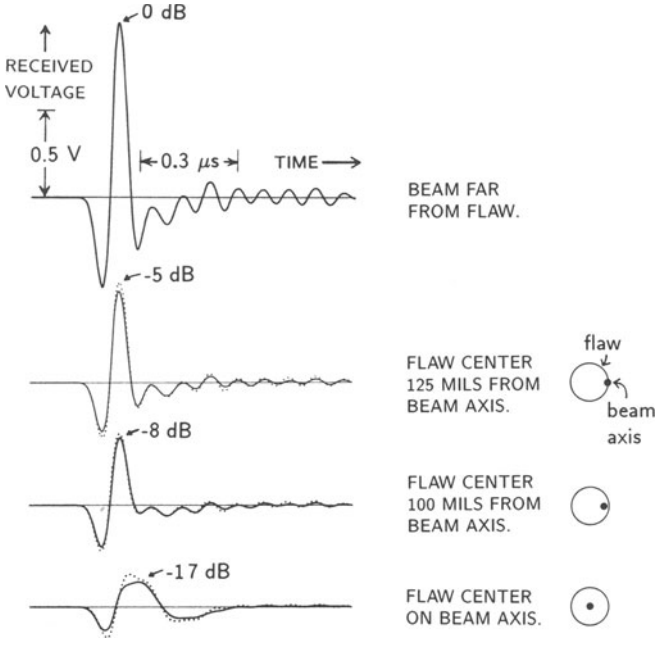

Fig. 3. Received voltage as a function of time when transmitting through a plate containing a 1/4"-diameter circular delamination. The same time and voltage scales are used for all four waveforms. (——): Experiment. (····): Theory with Gauss-Hermite beam model. Peak amplitude decibel values refer to the exp. signals.

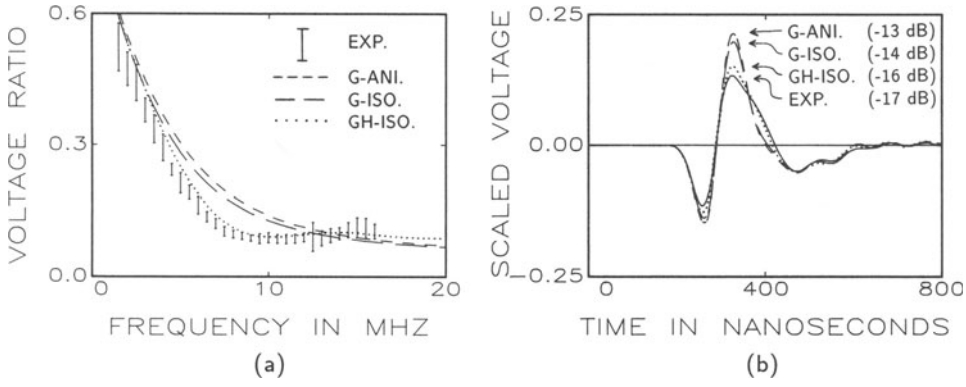

Fig. 4. Comparison of theory and experiment for 3/16" wide strip flaw centered on the beam axis. a) Experimental value of $\left|V_{flaw}(f)/V_{n.f.}(f)\right|$ compared with the predicted value of $\left|\Gamma_{flaw}(f)/\Gamma_{n.f.}(f)\right|$ as calculated using each of the three beam models. b) Experimental and predicted time-domain flaw signals, plotted on a scale where the peak amplitude of the no-flaw reference signal is unity. The single experimental signal shown was typical for flaws of this type. Peak amplitudes in decibels relative to the reference signal (0 dB) are also indicated.

we observe the effect of incorporating anisotropy into the Gaussian beam treatment. Comparing the lower two theory curves, we observe the effect of improving the beam model within the context of an isotropic treatment.

Figure 5a is typical of situations in which the beam is centered near an edge of a delamination of comparable size to the beam. Roughly 50% of the beam is blocked at all but the lowest frequencies, and there is little variation between the results of the three beam treatments.

The largest disagreements between theoretical and experimental voltage ratios were observed for 1/8" (.318cm) diameter circular flaws centered on the beam axis (Fig. 6). In this case, the flaw radius is less than half of the effective beam radius, and the theoretical voltage ratio is quite sensitive to the width of the central lobe of the beam profile. The Gauss-Hermite beam model with its sharper central lobe (see Fig. 2) is again in best agreement with experiment.

Amplitudes of time-domain signals are particularly important for industrial POD analyses, because change is amplitude is often the sole criterion used for flaw detection. Representative examples of experimental and predicted flaw signals are shown in Figs. 4b-6b. In general, the shapes of the predicted signals were found to closely mimic their experimental counterparts, but the predicted signal amplitudes tended to be a bit high. Amplitude errors of 1 to 2 dB were typical for the GH treatment, while errors of 2 to 4 dB were typical for the Gaussian beam treatments. The mean error in the latter case could be reduced by choosing a smaller initial width parameter, W_o. This would bring the Gaussian

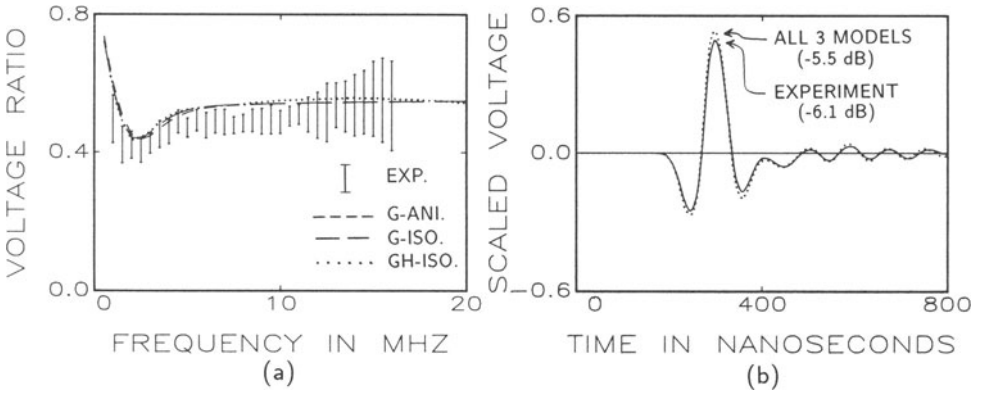

Fig. 5. Comparison of theory and experiment for 3/16" wide strip flaw. The center of the beam is 100 mils from the strip center, and thus is just inside the edge of the strip. See caption of Fig. 4. The three beam models lead to nearly identical results, and only the GH-predicted waveform is shown in panel b.

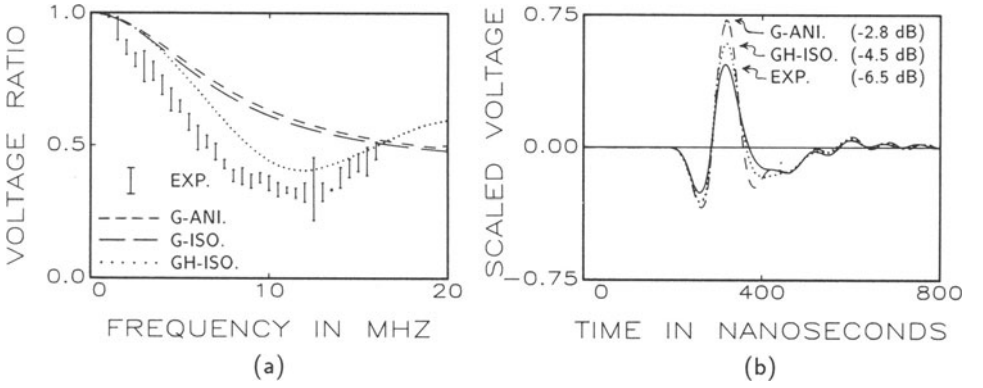

Fig. 6. Comparison of theory and experiment for 1/8" diameter circular flaw centered on the beam axis. See caption of Fig. 4.

beam profile into better agreement with the central lobe of the piston probe profile for the moderate values of $1<s<3$ characteristic of the experimental set-up.

CONCLUSIONS AND FUTURE WORK

The voltage ratio model based on Auld's reciprocity relationship offers a straightforward approach to predicting through-transmission, time-domain flaw signals. A key ingredient of the model is an experimental reference signal acquired through an unflawed portion of the plate. Equipment power levels, transducer properties, plate characteristics including layering and attenuation, and water/solid transmission coefficients all influence this reference signal and are encoded by it. The model then predicts the frequency-dependent modification of the reference signal caused by the presence of a delamination. Our initial experimental studies indicate that even simple versions of the

model may be sufficiently accurate to be of use in POD analyses of inspection systems.

The experimental studies to date have used planar transducers and an angle-ply layout. In these studies, the anisotropy of the composite plates did not have a pronounced effect on the through-transmitted signals. In the future we will investigate situations which emphasize the inherent anisotropy of composite materials, using, for example, uniaxial layouts, thicker plates, and focussed probes. As part of those studies, improvements in the model will be developed as dictated by the comparison of the existent model to experiment. Anticipated model developments include a GH treatment of the anisotropic case and an improvement on the Kirchhoff approximation.

ACKNOWLEDGEMENT

This work was sponsored by the Center for NDE at Iowa State University and was performed at the Ames Laboratory. Ames Laboratory is operated for the U.S. Department of Energy by Iowa State University under Contract No. W-7405-ENG-82.

REFERENCES

1. R. B. Thompson and T. A. Gray, J. Acoust. Soc. Am., 74, 1279 (1983).
2. T. A. Gray and R. B. Thompson, in, Review of Progress in Quantitative NDE, 5A, D. O. Thompson and D. E. Chimenti, Eds., (Plenum Press, NY, 1986), p. 911.
3. R. B. Thompson, D. O. Thompson, H. M. Burte, and D. E. Chimenti, in, Review of Progress in Quantitative NDE, 3A, D. O. Thompson and D. E. Chimenti, Eds., (Plenum Press, NY, 1984), p. 13.
4. R. B. Thompson and T. A. Gray, Phil. Trans. R. Soc. Lond. A320, 329 (1980).
5. R. B. Thompson and B. P. Newberry, "A model for the propagation of Gaussian beams in anisotropic media", these proceedings.
6. B. A. Auld, Wave Motion, 1, 3, 1979.
7. J. F. Nye, Physical Properties of Crystals (Oxford University Press, London, 1957), Appendix E.
8. R. B. Thompson and E. F. Lopes, J. Nondestrs. Eval. 4, 107 (1984).
9. R. B. Thompson and E. F. Lopes, in, Review of Progress in Quantitative NDE, 5A, D. O. Thompson and D. E. Chimenti, Eds., (Plenum Press, NY, 1986), p. 117.